Aerodynamic Design and Performance of a Bent-Axis Geometry Vehicle

W. H. Rutledge,* G. F. Polansky,* and E. L. Clark†
Sandia National Laboratories, Albuquerque, New Mexico

Variable bent-axis maneuvering vehicles provide a unique type of control for a variety of supersonic and hypersonic missions. Unfortunately, the large hinge moments often associated with these vehicles have prevented their application. This study examines the application of both experimental data and computational aerodynamics techniques in the design of such vehicles. A procedure is presented for the efficient design of a bent-axis geometry given a set of system constraints. In particular, the selection of vehicle parameters to produce minimum hinge moments for trimmed flight is examined in detail. Finally, the overall performance of the bent-axis geometry is reviewed in terms of static stability, lift-to-drag ratio, and control effectiveness.

Introduction

THE use of a bent-axis geometry is being considered for many applications because it provides a controlled lateral acceleration (e.g., a lift vector) with minimum impact on the thermal protection system of the vehicle. NASA has investigated the use of a bent-axis geometry for aerocapture missions as outlined by Walberg[1] and others.[2,3] These bent-axis, or "off-axis," geometries being considered by NASA are primarily intended for planetary entry and have a fixed bend for structural simplicity. However, a much more interesting design is one in which the amount of bend or deflection is adjustable during flight so as to regulate the magnitude of the lift vector. A simple variable bend body was considered by Larkin and Thomas[4] and Abzug[5] in a systems study that emphasized a high-g turning capability. In Larkin and Thomas' investigation, the inertia loads experienced in a constant high-g turn were used to compensate for the large hinge moments characteristic of bent-axis geometries. The current investigation will analyze the effect of hinge moments for trim and pseudotrim flight conditions during low-g maneuvers. Such conditions exist for extended range missions and boost-glide scenarios. During level flight and maneuvers involving low-g turns, hinge moments are dominated by aerodynamic forces. Therefore, inertia effects on the movable aft section will not be considered in this analysis.

The design of a bent-axis geometry for level flight missions is governed by the ability of the hinge actuators to overcome the aerodynamic hinge moments experienced by the movable aft section (i.e., tail section for this study). To date, this ability has been the major drawback to the application of variable bend geometries. This paper will demonstrate that, with the judicious selection of tail section length, these hinge moments can be controlled to within acceptable design specifications. In order to regulate the aerodynamic hinge moments to within manageable limits, tradeoffs are required between the tail section length, the total vehicle center of gravity (c.g.), and the deflection of the tail section. To minimize hinge moments, it is desirable to design the vehicle such that the tail deflection required for trim is close to the natural "free-floating" position of the tail section. It is this design procedure and the performance of the resulting geometry that are the subjects of this paper.

Presented as Paper 87-2491 at the AIAA Atmospheric Flight Mechanics Conference, Monterey, CA, Aug. 17-19, 1987; received Sept. 1, 1987; revision received March 22, 1988. This paper is declared a work of the U.S. Government and is not subject to copyright protection in the United States.

*Member of Technical Staff, Aerospace Projects Division. Senior Member AIAA.

†Member of Technical Staff, Experimental Aerodynamics Division. Associate Fellow AIAA.

The design of any maneuvering vehicle requires the analysis of aerodynamic data for the proposed class of vehicles at various control surface deflections. In the past, the only source for obtaining accurate data for control effectiveness was the wind tunnel. However, with the development of computational aerodynamics (CA) tools, it is now possible to eliminate much of the experimental design process in the wind tunnel. To use these CA tools with confidence, however, they must first be verified with experimental data. Once the designer is assured that the CA tool is predicting the correct aerodynamic behavior for the class of geometries of interest, the CA codes can be used to analyze small perturbations in geometry and flight conditions not available in the wind tunnel. The particular type of CA tools used in this analysis is based on an inviscid/boundary-layer formulation.

Computational Approach

Vehicle aerodynamics are predicted using inviscid flowfield and boundary-layer analysis. The inviscid and boundary-layer approach has been shown[6] to provide predictions of sufficient accuracy for a wide range of freestream conditions with considerably less computational effort than codes solving more complete forms of the governing equations; e.g., the parabolized Navier-Stokes codes.[7] Computational efficiency is especially important when studying parametric variations of vehicle geometry, such as the design study that follows.

The inviscid code used in the current study is the Sandia Inviscid Afterbody Code (SANDIAC). SANDIAC is an extension of the GE-3IS-SCM/ACM[8-10] code and is documented elsewhere.[11] The method incorporated in SANDIAC solves the three-dimensional, split coefficient matrix form of the Euler equations in a cylindrical base-coordinate system for an arbitrary three-dimensional grid. The use of a parabolic grid generator permits flowfield solutions for complex maneuvering geometries. This code also features a newly developed hybrid body boundary condition, which gives high accuracy and good crossflow shock-capturing capability.

The boundary-layer solutions are obtained by the Hypersonic Integral Boundary Layer Analysis of Reentry Geometries (HIBLARG) code. HIBLARG is a newly developed code similar in formulation to 3DMEIT[12] and applicable to complex geometries.[13] HIBLARG is a three-dimensional generalization of an existing two-dimensional technique.[14,15] The current code will solve spherically capped bodies with three-dimensional afterbodies subject to the limitations of the inviscid/boundary-layer formulation.

In the HIBLARG code, the integral forms of the momentum and energy equation are solved along the SANDIAC inviscid streamlines. Closure is achieved by specifying various boundary-layer parameters from correlations. The boundary-layer edge properties are determined by constructing a mass balance between the flow in the boundary layer and the local

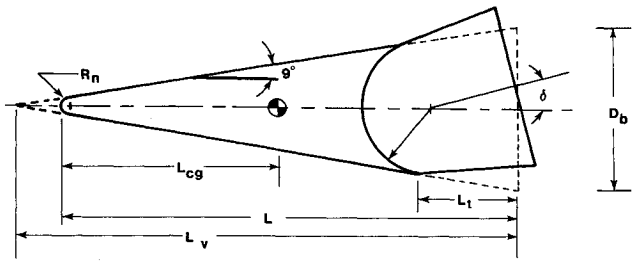

Fig. 1 Definition of bent-axis geometry.

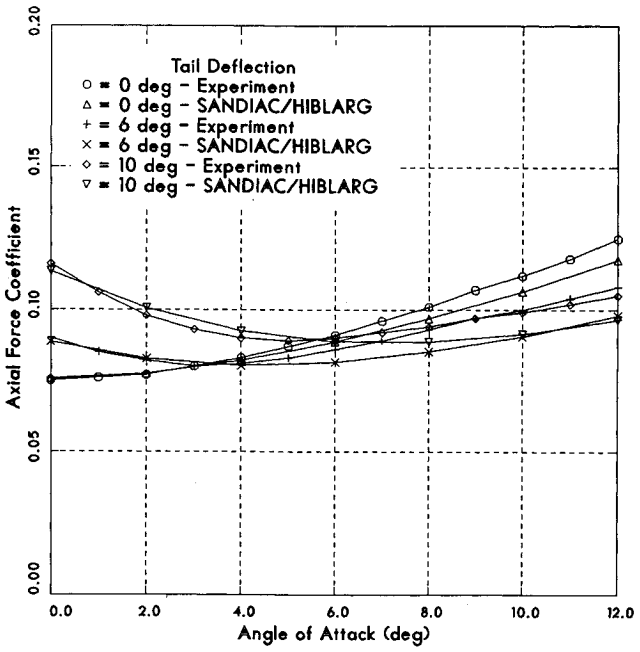

Fig. 2 Comparison of experimentally measured axial-force coefficient with predictions ($M=7.9$, $Re_\infty=4.9\times10^6$).

inviscid flowfield. The current formulation permits the calculation of either laminar or turbulent flow as determined by various transition criteria. However, for the current bent-axis geometry study, only turbulent boundary-layer conditions will be considered. This new inviscid/boundary-layer formulation of SANDIAC/HIBLARG has been demonstrated successfully on the NASA bent-axis configurations proposed for aerocapture missions.[16,17]

Validation

In order to establish an initial database for a bent-axis geometry, a force and moment wind-tunnel test was conducted on the geometry shown in Fig. 1. This test was performed in the Sandia National Laboratories Hypersonic Wind Tunnel at a Mach number of 7.9 and a unit Reynolds number of 4.9×10^6/ft. The wind-tunnel model was a 9 deg sphere-cone geometry with a nose radius of 0.175 in. and a total length of 10.105 in., giving a 10% nose bluntness ratio. The movable tail section was 20% of the vehicle virtual length. The nose of the model was gritted to ensure a turbulent flow over the model. The angle-of-attack range was from -5 to 16 deg with tail deflections of 0, ±2, ±6, and ±10 deg.

In the force and moment comparisons that follow, the reference length is the vehicle base diameter and the reference area is the vehicle base area. Angle of attack as well as the aerodynamic coefficients for the bent-axis vehicle are referenced to the axis of symmetry of the forecone. The moment reference point is also taken along this axis at a location of 57% of the physical length of the undeflected vehicle.

Figures 2-4 show comparisons of predicted values of axial-force, normal-force, and pitch-moment coefficients with experimental data for the vehicle with 0- to 10-deg tail deflection. The predicted values of normal-force coefficient and pitch-moment coefficient agree well with the experimental data across the angle-of-attack range. At higher bend angles, the difference between predicted and measured pitching moment results in a difference in trim angle of attack of about 1 deg. The predicted values of axial-force coefficient agree well with the experimental data for low angles of attack but fall somewhat below the data at higher angles of attack. This tendency to underpredict axial force at large angles of attack has been seen in previous studies[17] and possibly results from the inability of the inviscid/boundary-layer approach to predict crossflow separation on the leeward side of the vehicle. As the pitch-moment coefficient is of primary interest, these results are considered adequate for use in the current study. In order to cover a wider range of tail deflections than were tested in the experiment and to consider a vehicle with a different tail

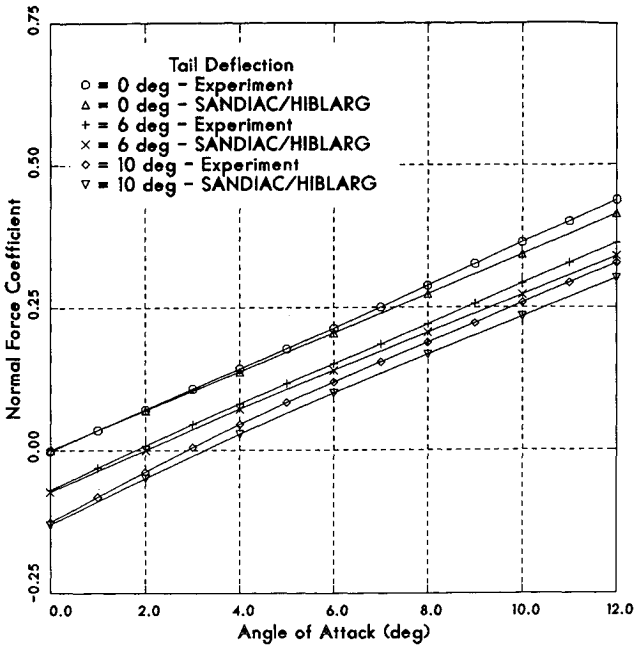

Fig. 3 Comparison of experimentally measured normal-force coefficient with predictions ($M=7.9$, $Re_\infty=4.9\times10^6$).

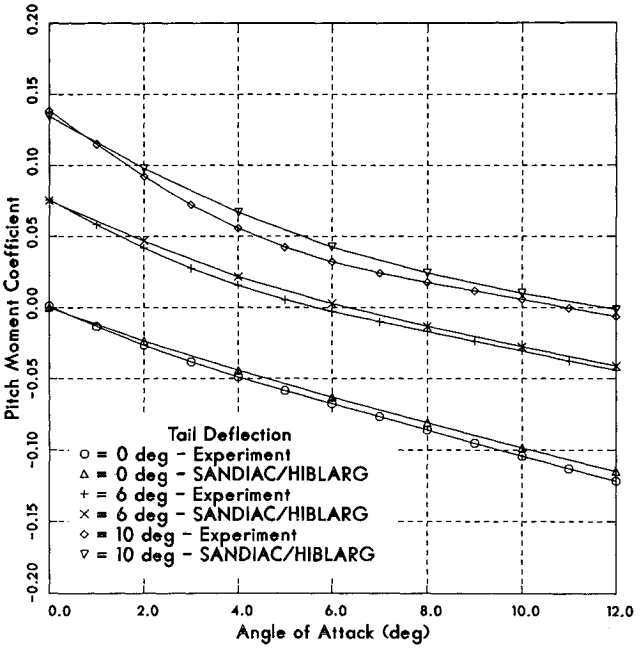

Fig. 4 Comparison of experimentally measured pitch-moment coefficient with predictions ($M=7.9$, $Re_\infty=4.9\times10^6$, c.g. = 57%).

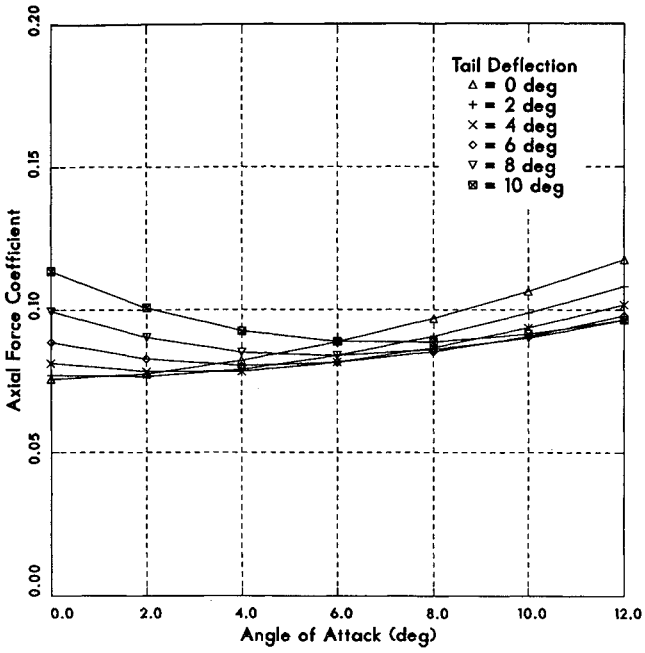

Fig. 5 Predicted values of axial-force coefficient for the 20% tail vehicle ($M=7.9$, $Re_\infty = 4.9\times10^6$).

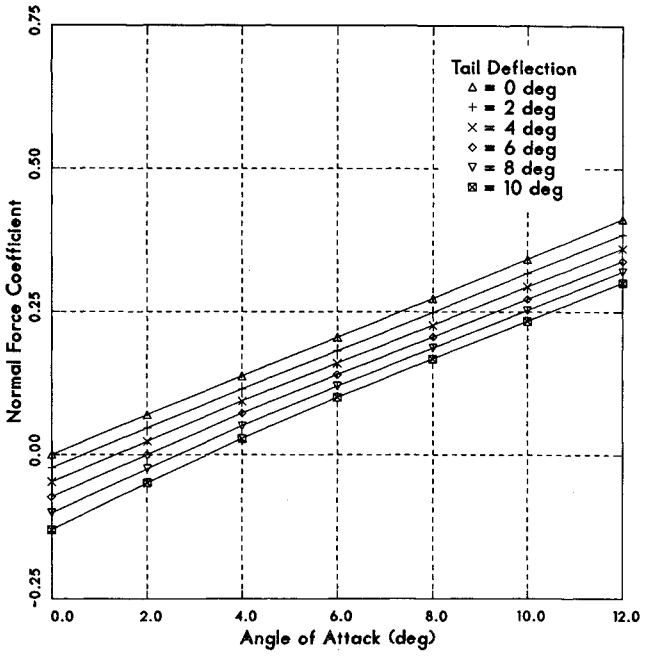

Fig. 6 Predicted values of normal-force coefficient for the 20% tail vehicle ($M=7.9$, $Re_\infty = 4.9\times10^6$).

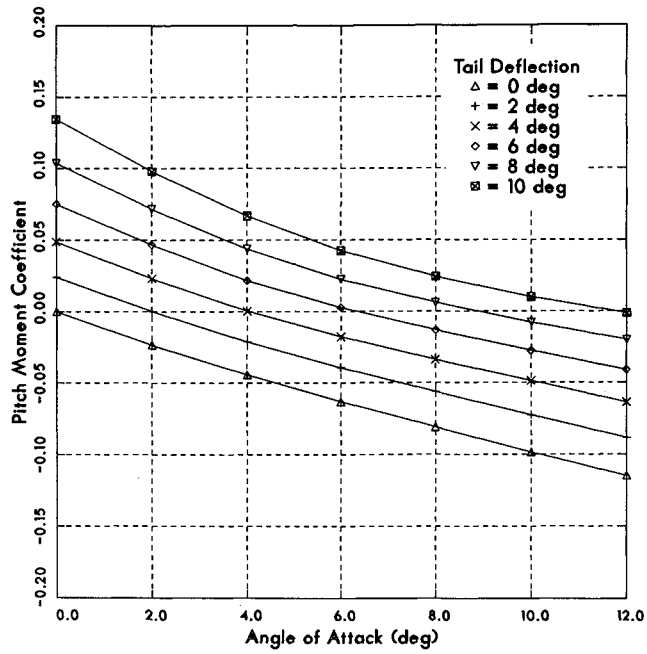

Fig. 7 Predicted values of pitch-moment coefficient for the 20% tail vehicle ($M=7.9$, $Re_\infty = 4.9\times10^6$, c.g. = 57%).

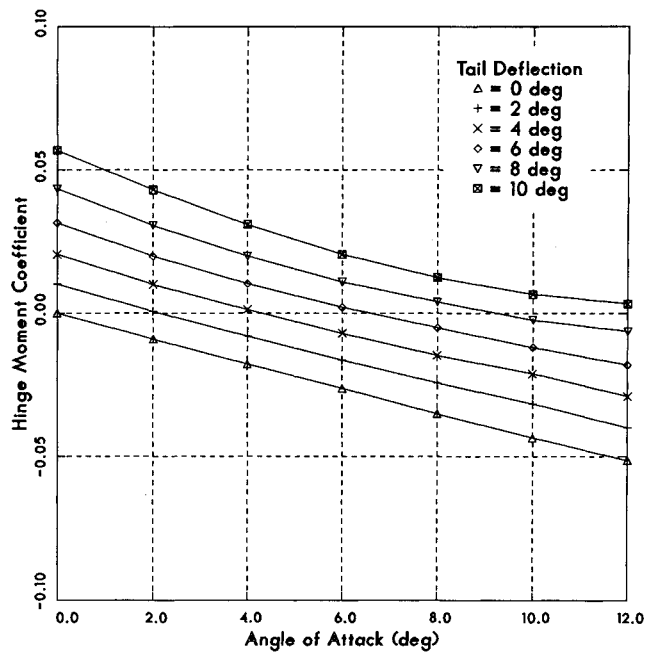

Fig. 8 Predicted values of hinge-moment coefficient about the hinge point for the 20% tail vehicle ($M=7.9$, $Re_\infty = 4.9\times10^6$).

section length, the computational results will be used in the studies that follow.

Design Considerations

For design purposes, two vehicles will be considered. The first vehicle is the 20% tail sphere-cone discussed previously. The predicted aerodynamics of the vehicle are summarized in Figs. 5–8, where predicted values of the axial-force, normal-force, pitch-moment, and hinge-moment coefficients are plotted as a function of both angle of attack and tail deflection. The pitch-moment coefficient is computed about a center-of-gravity (c.g.) location that is 57% of the physical length of the undeflected vehicle, giving a static margin of approximately 11%. Hinge moments are computed about the hinge location (i.e., the tail rotation point) and are determined by taking the difference in pitching moment between the baseline vehicle and a vehicle with no tail.

Table 1 Dimensions (in.) of bent-axis vehicles in this study

Tail, %	Nose radius, R_n	Total length, L	Virtual length, L_v	Tail length, L_t	Base diameter, D_b
10	0.175	10.105	11.049	2.2098	3.5
20	0.175	10.105	11.049	1.1049	3.5

The second vehicle is identical to the first, except that the tail length is 10% of the virtual length of the vehicle. The dimensions of the two vehicles are shown in Table 1. The predicted aerodynamics of this vehicle are summarized in Figs. 9–12, where predicted values of axial-force, normal-force, pitch-moment (about 57% c.g.), and hinge-moment coefficients are plotted as a function of both angle of attack and tail deflection.

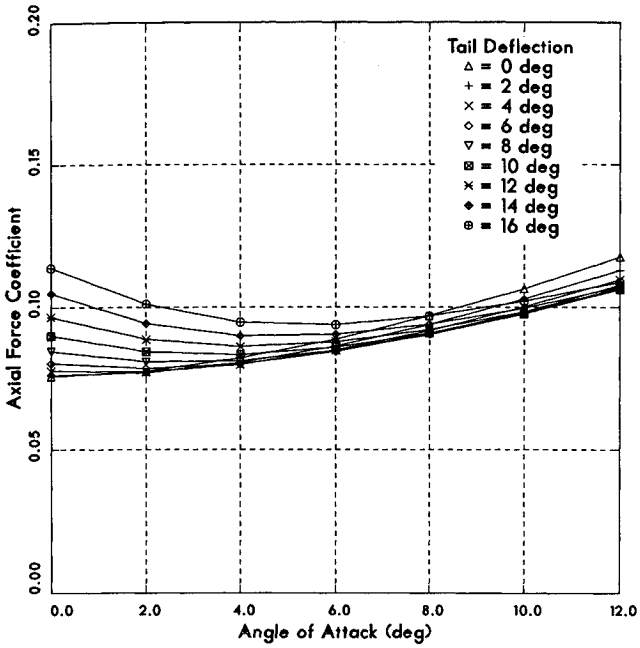

Fig. 9 Predicted values of axial-force coefficient for the 10% tail vehicle ($M=7.9$, $Re_\infty = 4.9\times10^6$).

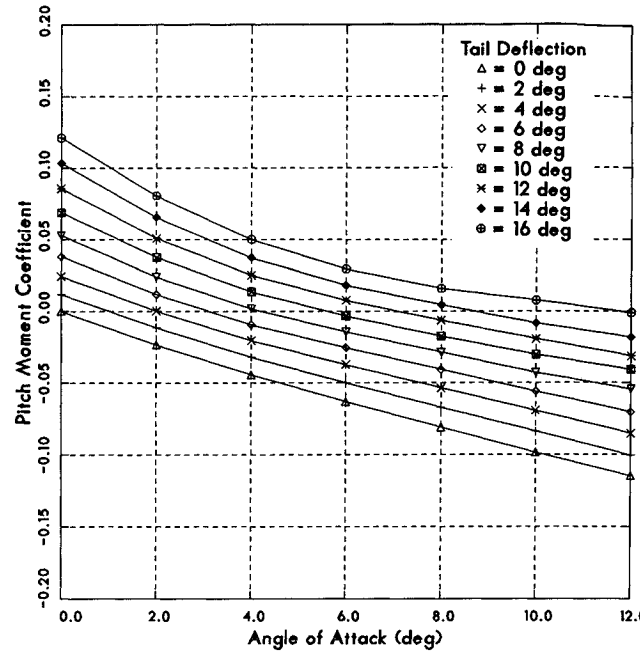

Fig. 11 Predicted values of pitch-moment coefficient for the 10% tail vehicle ($M=7.9$, $Re_\infty = 4.9\times10^6$, c.g. = 57%).

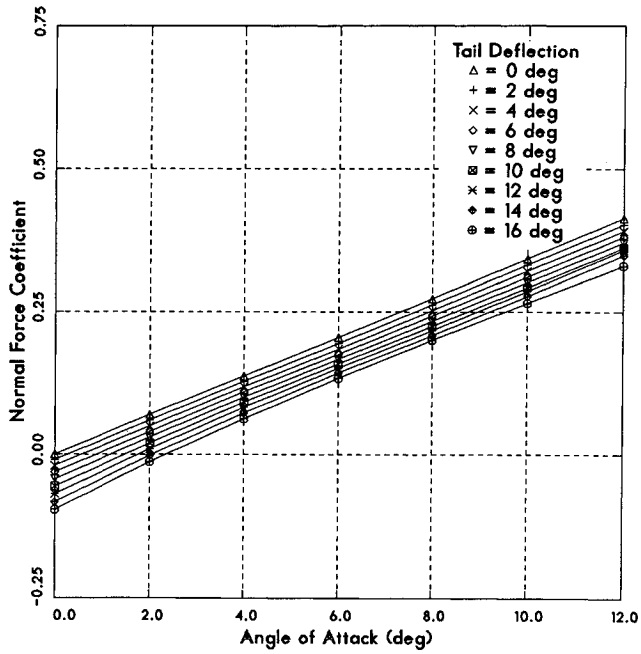

Fig. 10 Predicted values of normal-force coefficient for the 10% tail vehicle ($M=7.9$, $Re_\infty = 4.9\times10^6$).

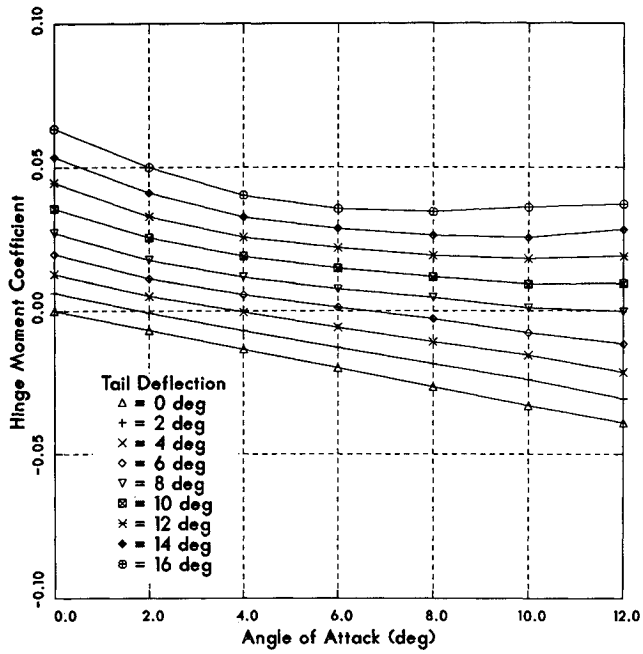

Fig. 12 Predicted values of hinge-moment coefficient about the hinge point for the 10% tail vehicle ($M=7.9$, $Re_\infty = 4.9\times10^6$).

As stated previously, hinge moments at trim conditions are often the driving consideration in the design of a variable bent-axis vehicle. The characteristics of the hinge-moment plots in Figs. 8 and 12 indicate that, for each value of angle of attack, there is a corresponding tail deflection that gives zero hinge moment. This is the "free-floating" position of the vehicle tail. If the vehicle trims at a specified angle of attack with the tail in the "free-floating" position, then this angle of attack can be maintained with zero hinge moment. The goal of the designer is to achieve this condition for a wide range of flight conditions.

The tail deflections required for trim angle of attack for 57% c.g. are shown in Fig. 13 for both the 10 and 20% tail vehicles. As would be expected, significantly larger tail deflections are required to trim the vehicle with the smaller tail. Figure 14 shows the corresponding hinge moments required to maintain trim conditions. As can be seen, the 20% tail vehicle is nearly optimum in the sense that hinge moments at trim are nearly zero across the angle-of-attack range. At 10-deg angle of attack, the hinge-moment coefficient required to trim the 10% tail vehicle is approximately 0.03. For flight conditions of Mach 20 at a 50,000-ft altitude (i.e., a freestream dynamic pressure of 68,200 psf) on a full-scale vehicle with a 24-in. base diam, the hinge moment would be over 150,000 in.-lb. At the same flight conditions, the hinge-moment coefficient required to trim the 20% tail vehicle is only -0.005, which gives a hinge moment of approximately 25,000 in.-lb. Clearly, there are tremendous gains in performance to be achieved through vehicle optimization.

As an indicator of the performance of the vehicles, Fig. 15 shows the lift-to-drag ratio at a trim angle of attack for the 10 and 20% tail vehicles. The lift-to-drag performance of the on-

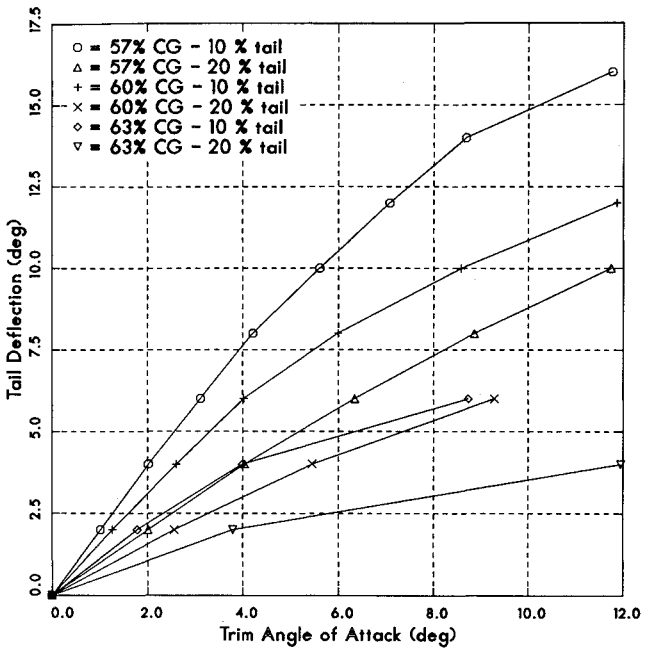

Fig. 13 Predicted values of tail deflection at trim angle of attack for both vehicles at various c.g. locations ($M=7.9$, $Re_\infty=4.9\times10^6$).

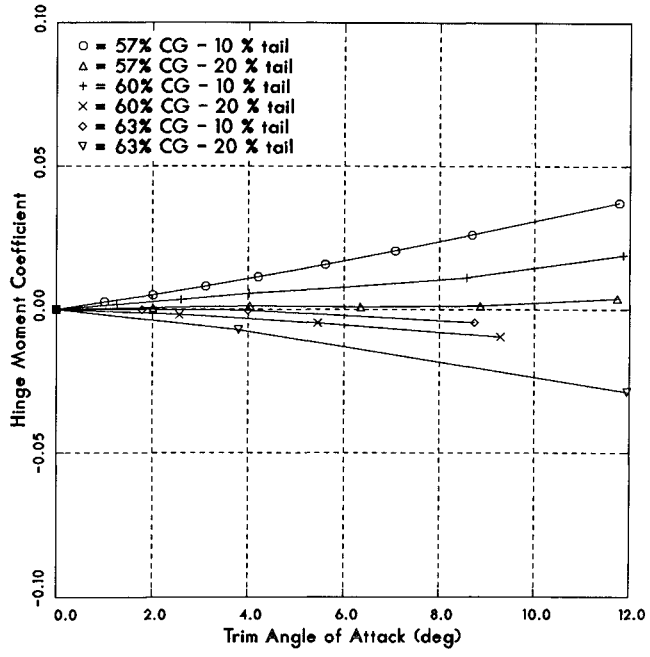

Fig. 14 Predicted values of hinge moment at trim angle of attack for both vehicles at various c.g. locations ($M=7.9$, $Re_\infty=4.9\times10^6$).

axis vehicle is included for comparison. The performance of the two bent-axis vehicles is nearly identical and considered good for a maneuvering re-entry vehicle.

We will now consider the effect of shifting the vehicle c.g. to 60% of the vehicle length (8% static margin). This produces an upward shift in the pitching-moment coefficient curves shown previously in Figs. 7 and 11. The deflections required to produce trim angle of attack at this c.g. are shown in Fig. 13, and the corresponding hinge-moment coefficients in Fig. 14. As expected, smaller tail deflections are required to produce an angle of attack for this lower static margin. The corresponding hinge moments for the 10% tail vehicle have decreased somewhat as compared to the previous case. However, the magnitude of the hinge moment has increased dramatically for the 20% tail case although the deflections are smaller. This is due to shifting the trim tail deflections from the optimum "free-floating" position.

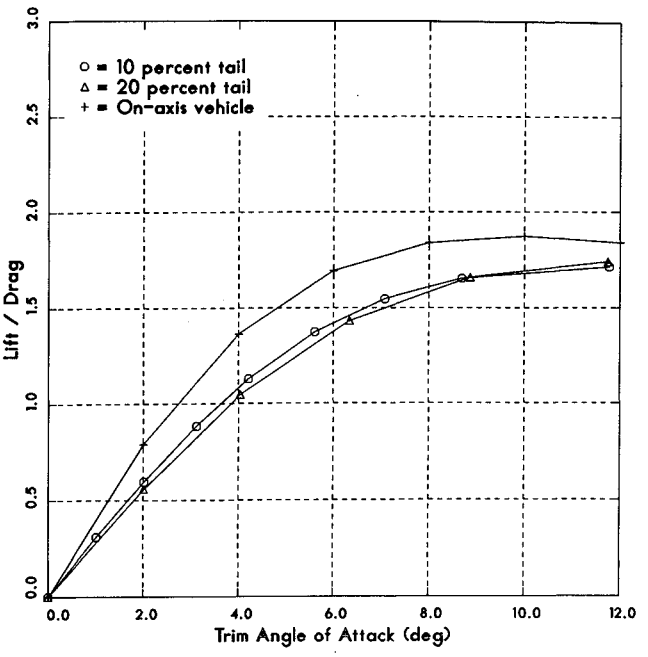

Fig. 15 Predicted values of lift over drag at trim angle of attack for both vehicles and for zero tail deflection ($M=7.9$, $Re_\infty=4.9\times10^6$, c.g. = 57%).

We will now consider another shift in the vehicle c.g. to 63% of the vehicle length (5% static margin). This produces a further upward shift in the pitching-moment coefficient curves shown previously in Figs. 7 and 11. The deflections required to produce trim angle of attack at this c.g. are shown in Fig. 13, and the corresponding hinge-moment coefficients in Fig. 14. Again, smaller tail deflections are required to produce angle of attack for this lower static margin. The corresponding hinge moments for the 10% tail vehicle are now nearly zero. This is the optimum c.g. for the 10% tail vehicle. Again, the magnitude of the hinge moment is increased for the 20% tail case although the deflections are smaller.

To achieve low hinge moments, the designer must be free to shift the vehicle c.g. for a fixed vehicle geometry or change the vehicle tail length if the c.g. is fixed. The vehicle can then be designed to trim with the tail near the "free-floating position" and the hinge moments reduced to very small values. Clearly, these designs can be optimized only for a single Mach number. Typically, the trim angle of attack is not a strong function of Mach number for bent-axis vehicles, therefore, these designs should give good performance over a reasonable range of flight conditions. In addition, it may be beneficial to select shorter-tail-length vehicles as the hinge-moment coefficient curves cross the zero value with a lower slope and should give better performance at off-design conditions.

Conclusions

A technique for minimizing the aerodynamic hinge moments associated with variable bent-axis geometry vehicles is described. To achieve this optimum, the designer must be free to shift the vehicle c.g. for a fixed vehicle geometry or change the vehicle tail length if the c.g. is fixed. The vehicle can then be designed to trim with the tail near the "free-floating position" and the hinge moments reduced to very small values.

References

[1]Walberg, G. D., "A Review of Aeroassisted Orbit Transfer," AIAA Paper 82-1378, Aug. 1982.

[2]"Generic Aerocapture Atmospheric Entry Study," Vol. 1: Final Report, General Electric Company and Jet Propulsion Laboratory, NASA CR-164160, Oct. 1980.

[3]"Generic Aerocapture Atmospheric Entry Study," Vol. 2: Trajectory Appendices, General Electric Company and Jet Propulsion Lab-

oratory, NASA CR-164160, Oct. 1980.
[4]Larkin, W. J. and Thomas, M., "Atmospheric Flight of a Variable-Bend Body," *Journal of Guidance and Control*, Vol. 2, Sept.-Oct. 1979, pp. 382-387.
[5]Abzug, M., "Hinged Vehicle Equations of Motion," AIAA Paper 80-0364, Jan. 1980.
[6]McWherter, M., Noack, R. W., and Oberkampf, W. L., "Evaluation of Inviscid/Boundary Layer and Parabolized Navier-Stokes Solutions for Design of Reentry Vehicles," *Journal of Spacecraft and Rockets*, Vol. 23, Jan.-Feb. 1986, pp. 70-78.
[7]Shanks, S. P., Srinivasan, G. R., and Nicolet, W. E., "AFWAL Parabolized Navier-Stokes Code: Formulation and User's Manual," Air Force Wright Aeronautics Laboratory, AFWAL-TR-82-3034, June 1982.
[8]Daywitt, J. E., Brant, D., and Bosworth, F., "Computational Technique for Three-Dimensional Inviscid Flowfields About Reentry Vehicles," Space and Missile Systems Organization TR-79-5, April 1978.
[9]Daywitt, J. E., Wade, M., Szostowski, D. J., and Yalisove, S., "Split-Coefficient Matrix Form of the GE-RSD Three-Dimensional Inviscid Supersonic Flowfield Code (3IS/SCM)," General Electric Co., GE 82SDR2029, April 1982.
[10]Daywitt, J. E., Szostowski, D. J., and Anderson, D. A., "A Split-Coefficient/Locally Monotonic Scheme for Multishocked Supersonic Flow," *AIAA Journal*, Vol. 21, June 1983, pp. 871-880.
[11]Noack, R. W., "Inviscid Flowfield Analysis of Maneuvering Hypersonic Vehicles Using the SCM Formulation and Parabolic Grid Generation," AIAA Paper 85-1682, July 1985.
[12]Murray, A. L. and Wolf, C. J., "Three-Dimensional Boundary Layers on Reentry Vehicles—Engineering Documentation and Users Manual," ACUREX Corp., ACUREX-FR-81-27/ATD, Dec. 1981.
[13]Kuntz, D. W., Polansky, G. F., and Buffington, R. J., "A Comparison of Predicted and Measured Aeroheating on a Reentry Vehicle Flap Geometry," AIAA Paper 87-0517, Jan. 1987.
[14]Dahm, T. J., Cooper, L., Rafinejad, D., Youngblood, S. B., and Kelly, J. T., "Passive Nosetip Technology (PANT II) Program—Volume I. Inviscid Flowfield and Heat Transfer Modeling for Reentry Vehicle Nosetips," SAMSO-TR-77-11, Space and Missile Systems Organizaton, Oct. 1976.
[15]Murray, A. L. and Saperstein, J. L., "User's Manual for the Updated ABRES Shape Change Code (ASCC 80)," Ballistic Missile Office, BMO/TR-80-52, Oct. 1980.
[16]Polansky, G. F. and Noack, R. W., "Inviscid/Boundary Layer Predictions of Aeroheating on a Bent-Axis Biconic," AIAA Paper 86-0303, Jan. 1986.
[17]Polansky, G. F. and Noack, R. W., "Inviscid/Boundary Layer Predictions of Aerodynamics for a Bent-Axis Biconic," AIAA Paper 86-2183, Aug. 1986.

Recommended Reading from the AIAA Progress in Astronautics and Aeronautics Series . . .

Spacecraft Dielectric Material Properties and Spacecraft Charging

Arthur R. Frederickson, David B. Cotts, James A. Wall and Frank L. Bouquet

This book treats a confluence of the disciplines of spacecraft charging, polymer chemistry, and radiation effects to help satellite designers choose dielectrics, especially polymers, that avoid charging problems. It proposes promising conductive polymer candidates, and indicates by example and by reference to the literature how the conductivity and radiation hardness of dielectrics in general can be tested. The field of semi-insulating polymers is beginning to blossom and provides most of the current information. The book surveys a great deal of literature on existing and potential polymers proposed for noncharging spacecraft applications. Some of the difficulties of accelerated testing are discussed, and suggestions for their resolution are made. The discussion includes extensive reference to the literature on conductivity measurements.

TO ORDER: Write AIAA Order Department, 370 L'Enfant Promenade, S.W., Washington, DC 20024
Please include postage and handling fee of $4.50 with all orders. California and D.C. residents must add 6% sales tax. All orders under $50.00 must be prepaid. All foreign orders must be prepaid. Allow 4-6 weeks for delivery.

1986 96 pp., illus. Hardback
ISBN 0-930403-17-7
AIAA Members $26.95
Nonmembers $34.95
Order Number V-107